Shear Assisted Electrochemical Exfoliation of Graphite to Graphene

Dhanraj B. Shinde[1], Jason Brenker[3], Rico F. Tabor[4], Adrian Neild[3], Mainak Majumder[1,2]

1. Nanoscale Science and Engineering Laboratory (NSEL), Mechanical and Aerospace Engineering, Monash University, Clayton, VIC-3800
2. Department of Chemical Engineering, Monash University, Clayton, VIC-3800
3. Laboratory for Micro-systems, Mechanical and Aerospace Engineering, Monash University, Clayton, VIC-3800
4. School of Chemistry, Monash University, Clayton, VIC-3800

Email: mainak.majumder@monash.edu

Abstract: The exfoliation characteristics of graphite as a function of applied anodic potential (1 to 10 V) in combination with shear field (400 to 74000 s^{-1}) has been studied in a custom-designed micro-fluidic reactor. Systematic investigation by atomic force microscopy (AFM) indicates that at higher potentials, thicker and more fragmented graphene sheets are obtained, while at potentials as low as 1 V, pronounced exfoliation is triggered by the influence of shear. The shear-assisted electrochemical exfoliation process yields large (~10 micron) graphene flakes with a high proportion of single, bi-layer, and tri-layer graphene, and small I_D/I_G ratio(0.21 to 0.32). This method comprises intercalation of sulphate and hydroxyl ions followed by exfoliation using shear induced by a flowing electrolyte. Our findings on the crucial role of hydrodynamics in accentuating the exfoliation efficiency suggests a safer, greener and more automated method for production of high quality graphene from graphite.

Graphene is the one atom thick 2D honeycomb sp^2 carbon lattice, which is attracting considerable attention for its potential application in next-generation composite materials, electronic and energy storage devices.[1] Since, the first report of monolayer graphene by Geim *et al.* produced using scotch tape[2], there has been sustained efforts to find alternative routes of production, both bottom up and top down. Ideally these should be scalable and capable of producing high quality graphene. Firstly, chemical vapor deposition (CVD) using gaseous precursors can be used to grow single graphene layers, however, the resulting properties are heavily dependent on the grain boundaries within the film and the high costs associated with this method would be a deterrent to large-scale industrial usage. Secondly, bulk graphite can be broken down into graphene flakes using a number of different methods, including intercalation of the graphite with reactive alkali metals, prolonged sonication and acid oxidation.[3-6] Whilst, the first two of these approaches can produce good quality graphene, they require long treatment times due to selectivity of reaction at the graphite-solvent interface and can cause reduction in the size of the graphene sheets produced.[4] The oxidation of graphite to graphene

oxide and the subsequent chemical, thermal or energetic reduction is currently the most popular method of production of graphene. It allows versatility, scalability, high yield and high dispersibility in a variety of solvents.[5, 6] The only concern is the inevitable generation of irreparable hole defects on the graphene sheets during oxidation, which sets a limit to the conductivity of the graphene. As such, there is an on-going search for alternative methods to produce defect-free, large-size graphene flakes.

A prime contender is the electrochemical exfoliation of graphite, which is fast and environmentally friendly.[7-9] However, graphite exfoliation, particularly at higher potential, results in over-oxidation, fragmentation and hole defects.[10-12]A recent study by Mullen *et al.* revealed that electrochemical exfoliation in ionic liquids results in graphene with small lateral size.[10] Furthermore, the graphene could be inadvertently functionalized with the ionic liquids used causing degradation of the electronic properties. Hence, the choice of electrolyte during the electrochemical exfoliation can play a major role in determining the composition, structure and properties of the resulting graphene sheets. Attempts to use acidic electrolytes to produce better quality graphene with larger lateral size[8, 10] have been hampered by the formation of oxygen-containing functional groups and fragmentation, which is inevitable given the high anodic potential (5- 10 V) utilized.

Given the appeal, but current limitations of the electrochemical techniques, our work focuses on using additional shear induced effects to enhance the quality of the graphene produced. Indeed, a recent report has suggested that efficient exfoliation occurred when local shear rate near a graphite interface exceeded a critical shear rate of $10^4\ s^{-1}$ in the absence of an electric field.[11] The interplay of hydrodynamics and electric fields has been historically studied by electrochemists for example in experiments using a rotating disk electrode.[12,13] Also several experiments describe the effects of forced convection, on the concentration, potential and current density distribution in an electrochemical micro reactor.[14] Oddly, no previous studies have examined graphite exfoliation in this manner. So, we have investigated how hydrodynamics impacts electrochemical graphite exfoliation, and delineated the role of the two physical parameters, applied shear and anodic potential, on the characteristics of the resulting graphene.

This investigation demonstrates that the synergy of shear with electrochemistry results in the formation of less defective and large-size sheets at a significantly lower potential of 1 V under a shear rate of $10^4\ s^{-1}$. Moreover this elegant flow reactor approach results in graphene sheets with very small I_D/I_G (ratio of Raman Intensity of defect to graphitic peaks) ratio of 0.21-0.35 and large lateral sizes of ~10 micron, in addition most of the graphene sheets are found to be in the form of single or bi-layers.

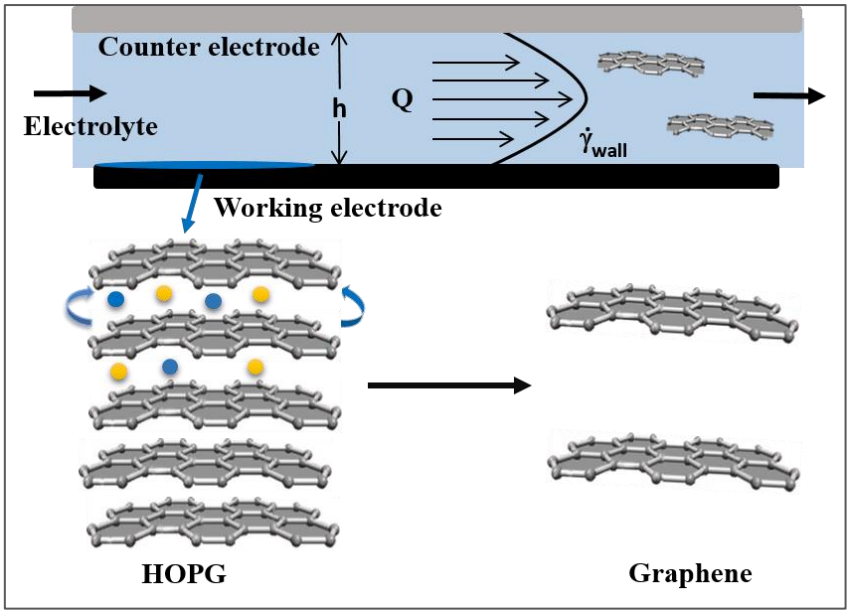

Figure 1: Schematic representation of the electrochemical micro-reactor showing the principles of our experiments. The graphite crystal is both the wall and the working electrode of the reactor and simultaneously experiences a high wall shear rate and an applied electric potential. Here h, Q and $\dot{\gamma}$ are the height between two electrodes, electrolyte flow and shear rate respectively.

Experiments were performed in a two electrode system using platinum as the counter electrode and highly ordered pyrolytic graphite, HOPG (SPI 1 grade, 10 mm × 10 mm ×0.2 mm), as the working electrode (depicted in Figure 1). In these experiments, 0.1 M H_2SO_4 was passed over the electrode with a high local shear rate, typically in the order of 10^2–10^4 s^{-1}. This was repeated for 170 cycles in a custom-designed micro fluidic cell, (As described in figure S1-S4). The potential applied was varied from 1 to 10 V. The shear rates reported here are computed from simulations of the fluid flow through the channel assuming a no slip boundary condition (figure S2), the values given are those which occur at the graphite electrode at a given flow rate.

Atomic force microscopy (AFM) was utilized as the primary method for size characterization of the resulting graphene samples, allowing statistical data on the lateral size and thickness distribution to be obtained.[15, 16] To do this, a graphene/ethanol suspension prepared from the exfoliated product was spin coated onto a glass surface. Raman spectroscopy was also used to investigate the defect density and the number of layers of the graphene sheets produced.

Figure 2 shows the mean flake size of the graphene sheets as a function of applied shear and potential. It can be seen that two distinct regions of exfoliation occurred. When the applied potential is in excess of approximately 4V the effect of shear rate, over the range investigated, on the mean flake size produced is minimal-exfoliation is electrochemically dominated. Below approximately 4V, variation in the resulting size is seen with respect to applied potential. In addition, it is in this region that the effect of shear rate, and so the possibilities offered by combining electrical and hydrodynamic

methods, is also clearly observed. At the two lowest potential levels used (1 and 2V), the synergy is further enhanced: in the absence of shear, and at a shear rate of 6925 s^{-1} no exfoliation was detected (appearing as a size of 0µm on the graph), exfoliation only becomes possible above a minimum shear rate level, and at that level the largest flakes are produced. This absence of exfoliation at low applied potential is in line with previous studies in which a minimum of 5V was required using electrochemical means alone.[10] To set the flake sizes reported here in context, the use of sonication yields flakes in the range of 300-900 nm and standard electrochemical methods result in flakes in the order of 1 micron.[10, 20]

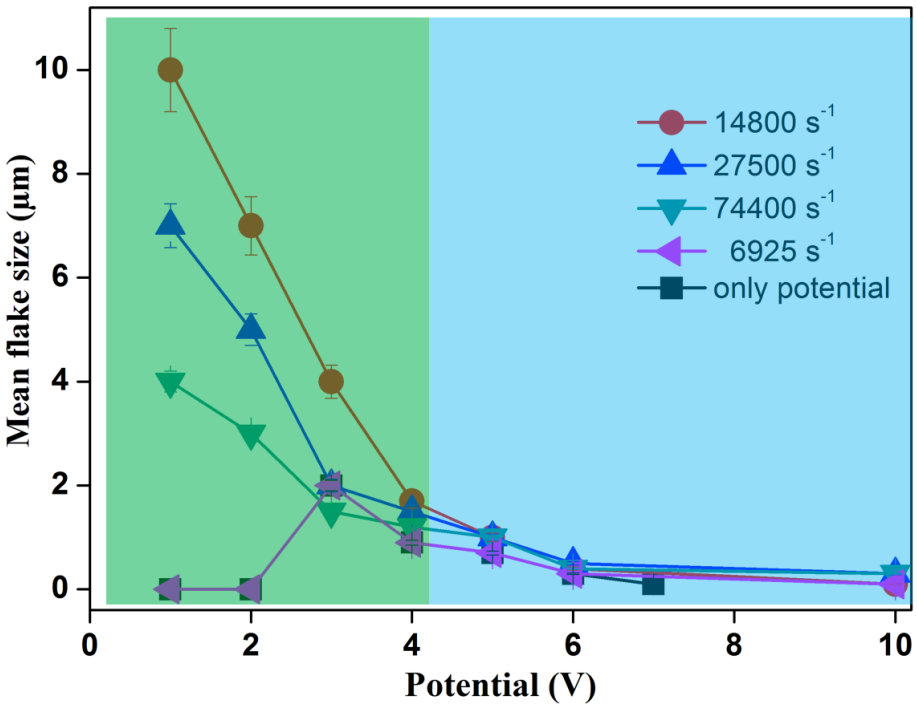

Figure 2: Effect of potential and shear rate on the size of graphene flakes produced in our flow reactor. A mean size distribution of zero, specifically in the cased for only potential and shear rate of 6925 s^{-1}, indicates that exfoliation was unnoticed over the samples that were measured. The green and blue colour in the figure indicates shear and potential dominated regions, respectively.

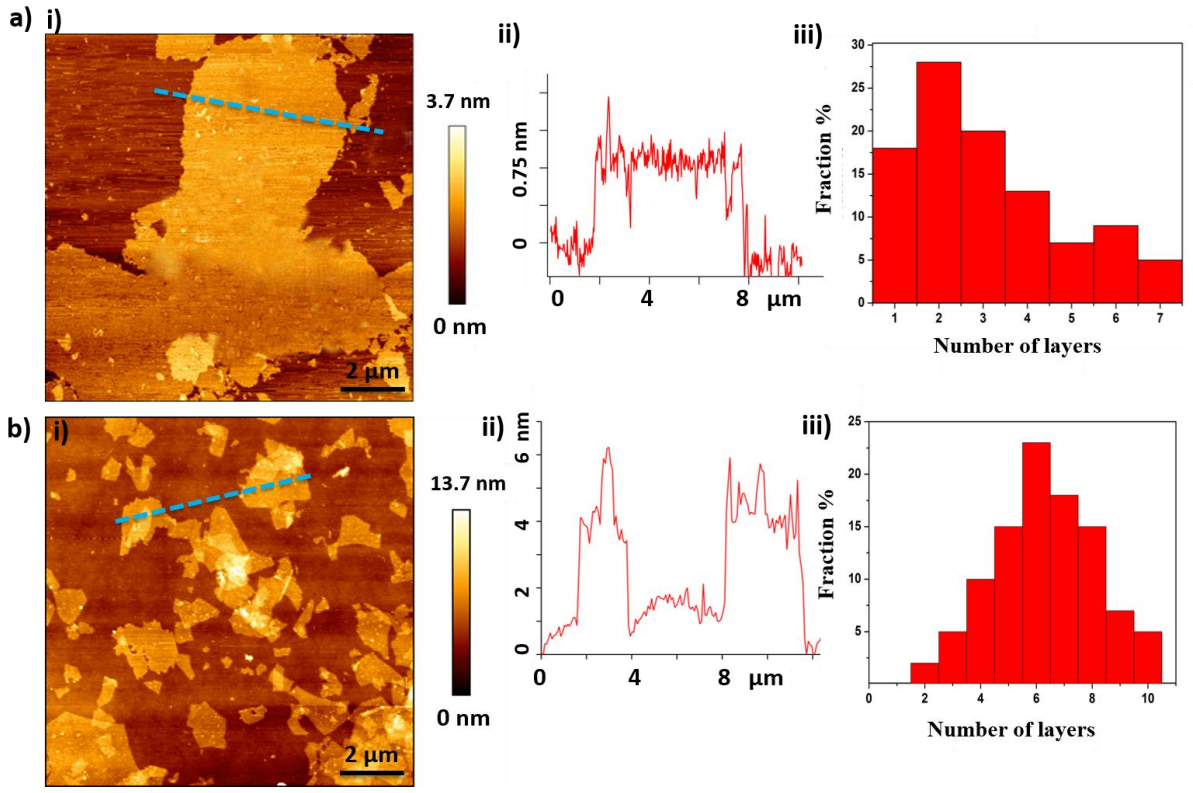

Figure 3: AFM measurement of the graphene sheets showing lateral dimensions (i), height profile (ii) and a histogram of layer thickness for 80 graphene sheets (iii). These data has been provided for (a) 1V applied potential and a shear rate of 27500 s^{-1}, (b) 5V applied potential at the same shear rate.

In figure 3, we show representative AFM measurements for exfoliated products obtained at 1V applied potential in combination with 27500 s^{-1}. The statistical thickness analysis shows that most of the graphene layers are either monolayers, with about 16% of the sheets lower than 0.8 nm with more than 75% of the flakes have a thickness of less than 4 layers.[18] In contrast to this excellent exfoliation outcome, when the potential is increased (data from 5V is shown in Figure 3b) while maintaining the same shear rate, the process yielded not only smaller sheets, as was seen in figure 2, but also thicker sheets, the average size being 6-8 layers (Figure S5-S7 shows further example of lateral dimensions of graphene sheets using transmission electron microscopy and AFM).

To quantitatively examine the defect density and quality of graphene, the samples were studied using Raman spectroscopy as shown in figure 4. Raman spectra shows three peaks: the D band around 1350 cm^{-1}, the G band around 1590 cm^{-1} and the 2D band (the overtone of the D band) around 2700 cm^{-1}. The G band represents the in-plane bond-stretching motion of the pairs of carbon sp^2 atoms, while the intensity of D band is directly related to the amount of defects present in the graphene sheets.[21] As exfoliation potential increases from 1 to 10V, I_D/I_G ratio of the samples increases from 0.1 to 0.8, indicating that higher structural order is retained at lower exfoliation potential, noting that a shear rate above 6925 s^{-1} is required to initiate exfoliation. Once again to bring the I_D/I_G ratio into context, electrochemical techniques typically yields ~0.5, while pure shear

exfoliation yields ~0.7,[10, 11] our values are as low as 0.21, whilst HOPG, with its very low defect density, has a value of 0.004. The I_{2D}/I_G ratio, a measure of layer thickness[21-22], exhibited an increase with shear rate at a given potential as shown in figure 4a. The change in shape, shift of peak position to lower wave number and increased band intensity graphene of the 2D band in our samples indicate that thin graphene sheets are produced (Figure 4a). This information is further analysed in figure 4c, which shows that the thinnest sheets are obtained by using a low potentials (1-4 V). This trend is also confirmed by AFM data as shown in Figure 4c. Hence the detrimental effect of the application of higher potential on the sheet size (figure 2), defect concentration (figure 4b) and thickness (figures 3 and 4c) in the graphene sheet is unambiguously demonstrated.

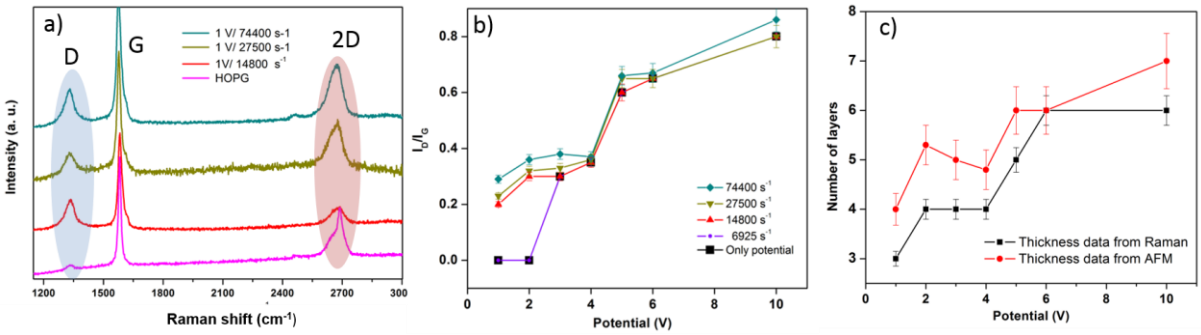

Figure 4. Raman spectra of graphene sheets in the D, G and 2D band regions. a) Representative Raman spectra shows presence of single to few layer graphene for samples prepared at 1V potential by changing shear rate; (b) The variation in the I_D/ I_G ratios with shear rate at applied potential. c) Number of layers calculated from the ratio of I_{2D}/I_G ratio from the Raman spectra shows excellent agreement with AFM thickness data. The data is averaged over all the shear rates used, the error bars demonstrate relatively small alteration in thickness as a function of this parameter.

Combining the information gathered on the geometric features of the flakes produced three trends are now examined. The trend 1 is that at a given potential there is little variation in the thickness of the graphene flakes produced with shear rate used (figure 4c – small error bars despite averaged over all shear rates). However, as the potential is increased, the trend 2 is that the flakes become both thicker (figure 4c) and smaller (Figure 2). Finally, the trend 3 is that at low potential, a low shear rate (above a certain minimum value such that exfoliation occurs) yields large flakes (Figure 2).

In considering the trend 1, it is known that the application of potential introduces defects in the form of oxygenated groups to the graphene,[10] we hypothesize that the level of potential influences the depth of intercalation of the ions into the working electrode and as such controls the exfoliated flake thickness, as such shear would play slight role in determining this parameter.

A simple film tearing model can then link this thickness relationship with the lateral dimensions of the flakes created (trend 2). The tearing of adhered films has been studied in depth at the macroscale[23], and this theory has recently been applied to the removal of graphene sheets from a

substrate.[24] The propagation of the tear can be considered by examining the energies associated with elastic deformation (of the film bent double in the vicinity of the tear), fracture and adhesion. Through energy minimisation, it can be shown that the forces present on one half of the symmetric film are as shown in figure S8. The key forces are: (a) $\tau W/2$, which is the adhesive energy dissipation as the film is de-adhered, τ being the adhesive energy, and W the width of the tear. (b) γt the fracture force, γ is the work of fracture and t is the film thickness. (c) $\partial U_E/\partial W$ which is the lateral elastic energy gradient, a force arising from the minimisation of energy (as the film width is reduced) related to the bending energy of the film at the tear, U_E. The lateral elastic energy gradient in turn can be equated to $4BW/h$, where B is the bending modulus and h the height of the torn film above the substrate. Where the height (h) is given by

$$h^2 = -8\frac{\partial \mathrm{h}}{\partial \mathrm{x}}\frac{B}{\tau}$$

in the case of a steadily pulled film. And finally, (d) F which is the pulling force applied to tear the film. Taking these expressions together and completing a force balance yields.[23]

$$F = \tau\frac{W}{2} + \gamma t cos\theta \quad (1)$$

$$\frac{\partial U_E}{\partial W} = \gamma t sin\theta \quad \text{or} \quad \frac{\sqrt{2B\tau}}{\eta} = \gamma t sin\theta \quad (2)$$

where $\eta^2 = -\partial h/\partial x$, and is 1 for a torn film which is bent over a cylindrical profile.

The analysis, performed on macroscale films, is for constant velocity of the tip of the unpeeled part of the film. In our shear driven system, the driving force is yielded by the boundary condition describing the degree of slip on the untethered flap. As such, the force available depends on a range of factors including the unpeeled area, and the shear rate at the boundary ($F = A\mu\gamma$, where A is the torn flap area, μ is the viscosity and γ is the shear rate). The combination of these factors, make a full model beyond the scope of this manuscript, however, this simple analysis shows agreement with the experimental data. Namely, through equation 2, a link can be made between thickness of film, t, and angle of crack propagation, θ. With the bending modulus proportional to thickness cubed,[23] a thicker film corresponds to a larger angle (the second expression in equation 2 gives: $\sqrt{t} \propto sin\theta$), and as such a smaller flake (see figure S8).

Trend 3 is that once sufficient shear rate is present to cause flakes to be removed from the substrate at low potential, there is a clear tendency to have reduced flake size as the shear is increased. Two mechanisms exist which can explain this, the first is that the flakes may be broken in the more extreme flow conditions, post removal. The second is related to the tearing of the flake from the substrate. As the shear rate is increased more force is applied to the flake as it is being removed, this excess force will cause the removal to become more rapid. As the speed of tearing increases, a link has been proven with increasing adhesion energy, τ, in the macroscale.[23] If a similar phenomenon, one which is poorly understood presently, is applicable to the removal of graphene flakes, this would lead to an increase in crack propagation angle (the second expression in equation 2 yields $\sqrt{\tau} \propto sin\theta$), and

as such a reduction of flake size. A simple analogy can be made to the removal of sticky tape, when pulled quickly a small triangular piece is ripped off, to remove a whole piece the patience to pull the tape off slowly and gently is required.

Whilst this film tearing model has been developed for a considerably simpler system than ours, it is sufficient to link two observed trends (2 and 3) in the low potential regime in which shear rate clearly plays a role in flake removal: an increase of thickness due to higher applied potentials leads to smaller flake size; and at a given potential a higher shear rate leads to a smaller flake size.

Through the use of hydrodynamic shear, we have opened up the possibility of exfoliation at a lower potential level than possible in the absence of shear. Consequently, fragmentation and over-oxidation of graphene sheets was minimised leading to less defective exfoliation of graphite to graphene. Raman fingerprints for single-, bi-, and few-layer graphene reflect changes in the electronic structure and allow explicit, non-destructive identification of graphene layers complement AFM studies, which provides information regarding the average size and lower thickness of graphene sheets synthesized at lower potential with optimized shear rate. As such a new regime of exfoliation has been characterised in which low defect, large and thin flakes can be produced using modest shear and low potentials. Our approach of utilizing flow chemistry in exfoliating graphite, which couples mechanical and electrochemical exfoliation, allows the preservation of the graphene chemistry at the molecular scale and possess exciting elements such as the ability to be automated with far less difficulty than batch reactions, avoidance of size reduction through the use of low potential during exfoliation, and offers the possibility of introducing multi-step reactions such as functionalization with other chemicals in a continuous sequence.

In conclusion, we have for the first time demonstrated the role of hydrodynamics in a shear-assisted electrochemical exfoliation approach, effectively reducing defect density and fragmentation. Thin layer graphene with large flake size was obtained at lower potentials, demonstrating the great opportunity for shear-assisted electrochemical exfoliation of few layer graphene from graphite. These results could instigate the development of environmentally benign, safe, and efficient methods for the exfoliation of other 2D materials for a variety of applications.

References:

1. Y. Wang, X. Chen, Y. Zhong, F. Zhu and K. P. Loh, *Appl. Phys. Lett.*, 2009, **95**, 063302.
2. K. S. Novoselov, A. K. Geim, S. V. Morozov, D. Jiang, Y. Zhang, S. V. Dubonos, I. V. Grigorieva and A. A. Firsov, *Science*, 2004, **306**, 666.
3. P. W. Sutter, J. I. Flege and E. A. Sutter, *Nat. Mater.*, 2008, **7**, 406.
4. Z. Y. Xia, S. Pezzini, E. Treossi, G. Giambastiani, F. Corticelli, V. Morandi, A. Zanelli, V. Bellani and V. Palermo, *Advanced Functional Materials*, 2013, **23**, 4684-4693.
5. W. S. Hummers and R. E. Offeman, *J. Am. Chem. Soc.*, 1958, **80**, 1339.
6. D. C. Marcano, D. V. Kosynkin, J. M. Berlin, A. Sinitskii, Z. Sun, A. Slesarev, L. B. Alemany, W. Lu and J. M. Tour, *ACS Nano*, 2010, **4**, 4806-4814.
7. J. H. Lee, D. W. Shin, V. G. Makotchenko, A. S. Nazarov, V. E. Fedorov, Y. H. Kim, J. Y. Choi, J. M. Kim and J. B. Yoo, *Adv. Mater.*, 2009, **21**, 4383.
8. K. Parvez, R. J. Li, S. R. Puniredd, Y. Hernandez, F. Hinkel, S. H. Wang, X. L. Feng and K. Müllen, *ACS Nano*, 2013, **7**, 3598.
9. D. B. Shinde, J. Debgupta, A. Kushwaha, M. Aslam and V. K. Pillai, *Journal of the American Chemical Society*, 2011, **133**, 4168-4171.
10. K. Parvez, Z.-S. Wu, R. Li, X. Liu, R. Graf, X. Feng and K. Müllen, *Journal of the American Chemical Society*, 2014, **136**, 6083-6091.
11. K. R. Paton, E. Varrla, C. Backes, R. J. Smith, U. Khan, A. O'Neill, C. Boland, M. Lotya, O. M. Istrate, P. King, T. Higgins, S. Barwich, P. May, P. Puczkarski, I. Ahmed, M. Moebius, H. Pettersson, E. Long, J. Coelho, S. E. O'Brien, E. K. McGuire, B. M. Sanchez, G. S. Duesberg, N. McEvoy, T. J. Pennycook, C. Downing, A. Crossley, V. Nicolosi and J. N. Coleman, *Nat Mater*, 2014, **13**, 624-630.
12. N. Rodríguez Muñoz, J. Hinojosa Palafox and K. Kohlhof, in *Sustainability in Energy and Buildings*, eds. R. Howlett, L. Jain and S. Lee, Springer Berlin Heidelberg, 2011, vol. 7, ch. 10, pp. 91-99.
13. H. A. Gasteiger, N. M. Markovic and P. N. Ross, *The Journal of Physical Chemistry*, 1995, **99**, 8290-8301.
14. Yoshida and Jun-ichi., *The Electrochemical Society Interface*, 2009, **40**.
15. L. M. Malard, M. A. Pimenta, G. Dresselhaus and M. S. Dresselhaus, *Phys. Rep.*, 2009, **473**, 51.
16. Q. K. Yu, L. A. Jauregui, W. Wu, R. Colby, J. F. Tian, Z. H. Su, H. L. Cao, Z. H. Liu, D. Pandey, D. G. Wei, T. F. Chung, P. Peng, N. P. Guisinger, E. A. Stach, J. M. Bao, S. S. Pei and Y. P. Chen, *Nat. Mater.*, 2011, **10**, 443.
17. C. Y. Su, A. Y. Lu, Y. P. Xu, F. R. Chen, A. N. Khlobystov and L. J. Li, *ACS Nano*, 2011, **5**, 2332.
18. Z. G. Cheng, Q. Y. Zhou, C. X. Wang, Q. A. Li, C. Wang and Y. Fang, *Nano Lett.*, 2011, **11**, 767.
19. D. B. Shinde, M. Majumder and V. K. Pillai, *Scientific reports*, 2014, **4**, 4363.
20. A. M. Abdelkader, I. A. Kinloch and R. A. W. Dryfe, *ACS Applied Materials & Interfaces*, 2014, **6**, 1632-1639.
21. R. John, D. B. Shinde, L. Liu, F. Ding, Z. Xu, C. Vijayan, V. K. Pillai and T. Pradeep, *ACS Nano*, 2014, **8**, 234-242.
22. C. Cong, T. Yu, R. Saito, G. F. Dresselhaus and M. S. Dresselhaus, *ACS Nano*, 2011, **5**, 1600-1605.
23. E. Hamm, P. Reis, M. LeBlanc, B. Roman and E. Cerda, *Nat Mater*, 2008, **7**, 386-390.
24. D. Sen, K. S. Novoselov, P. M. Reis and M. J. Buehler, *Small*, 2010, **6**, 1108-1116.

Supporting Information

Shear Assisted Electrochemical Exfoliation of Graphite to Graphene

Dhanraj B. Shinde[1], Jason Brenker[3], Rico F. Tabor[4], Adrian Neild[3], Mainak Majumder[1,2]

1. Nanoscale Science and Engineering Laboratory (NSEL), Mechanical and Aerospace Engineering, Monash University, Clayton, VIC-3800
2. Department of Chemical Engineering, Monash University, Clayton, VIC-3800
3. Laboratory for Micro-systems, Mechanical and Aerospace Engineering, Monash University, Clayton, VIC-3800
4. School of Chemistry, Monash University, Clayton, VIC-3800

Email: mainak.majumder@monash.edu

Contents

S1. Experimental Design of Reactor and Assembly

We were able rapidly prototype designs of the micro-reactor by using 3D printing, modifying the shear rate within the channel was accomplished by printing a new channel for each shear rate required. The limiting factors were the maximum volumetric flow rate of the syringe pumps used ($6.242 \times 10^{-7} m^3.s^{-1}$) the minimum cross sectional area produced by the 3D printer ($4 \times 10^{-8} m^2$). CAD models of each component were produced taking into account the need to install electrodes within the channel whilst ensuring a sealed final device. This was achieved by utilising multiple materials in a Stratsys Objet 350 Connex 3D printer. Vero White was used as the interior of the channel and structural components and Tango Black to form seals between component layers. Implementing potential and shear is possible through a well-designed continuous flow reactor, which is linked to four syringes (Terumo, 12ml) on a syringe pump (figure S1), which pumps electrolyte through a very narrow channel at a constant shear rate (table S1). Sandwiched between electrochemical cell is a piece of highly ordered pyrolytic graphite, (HOPG), with Pt wire as counter electrode, placed parallel to the working electrode as shown in details (Figure S5).

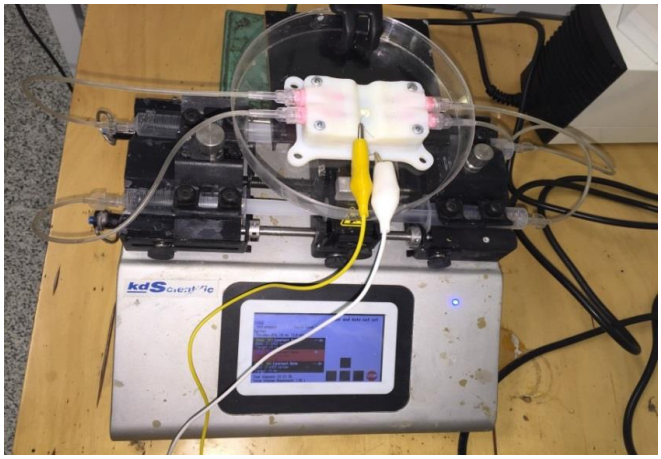

Figure S1: Photograph of the experimental set-up.

In order to optimise the shear rate within the working section of the device a 3D computational model was produced in COMSOL Multiphysics software. These models took into account the variations in height (distance between electrodes) and width of each channel as well as the two flow rates investigated. Models were simplified by only simulating the working sections, the 10 mm length of channel over the working electrode. The laminar flow module was selected considering the relatively low Reynolds numbers achieved during these experiments.

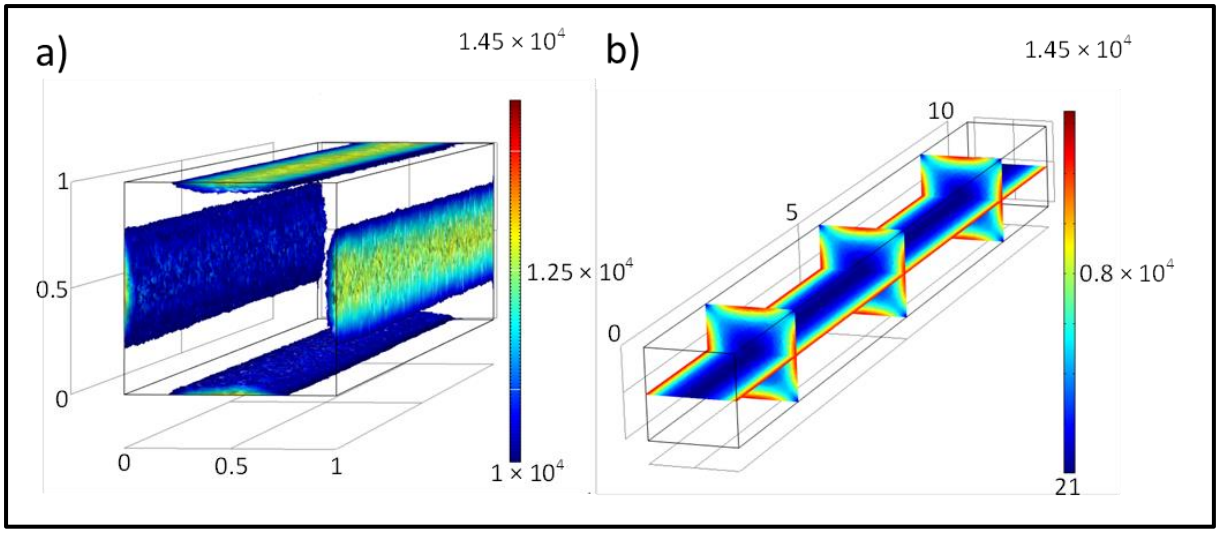

Figure S2: a) The iso-surface plots of the regions near the walls where exfoliation by shear occurred, b) slices indicating the shear rate distribution throughout the channel. The channel lengths are in mm and shear rate is in s^{-1}.

Table S1: Design parameters showing the dimensions of the channels, and maximum shear rate generated in the electrochemical micro-reactor:

Channel Dimensions (mm)		**No. of Syringes**	**Local Shear Rate (s^{-1})**
Height	**Width**		
1	10	1	446
0.5	10	1	1692
1	10	2	859
0.5	10	2	3340
1	1	1	6925
1	1	2	14800
0.5	1	1	27,500
0.5	1	2	74,400

For each electrochemical exfoliation experiment the experiment, 8 ml of electrolyte (0.1M H_2SO_4) was used. Drawing only 8ml of electrolyte will ensure that there is no pressure build up in the channel width that could potentially trigger a leakage. After, each experiment with specific combination of potential and shear rates, samples were collected from all syringes into a vial and washed carefully using dialysis (cellulose membrane having pore size in the range of 1-10 nm) to remove the salt contain before any further characterization.

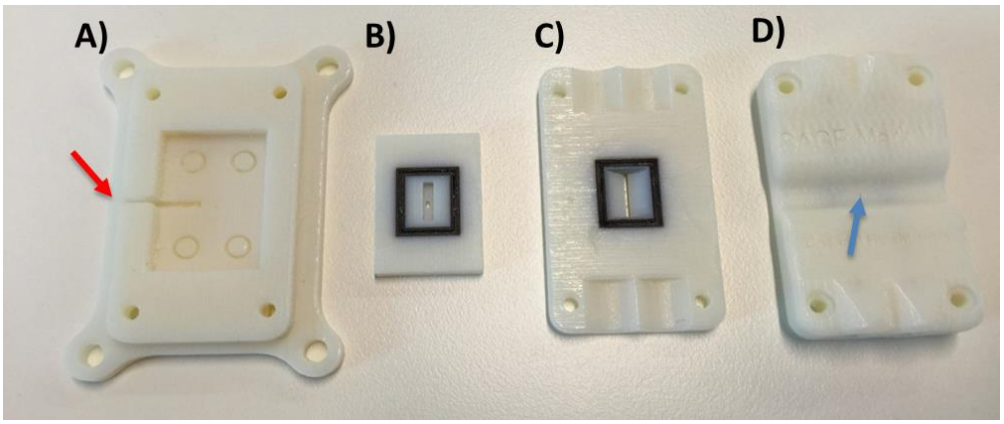

Figure S3: A: Reactor cell base contains the platinum foil, which comes in contact with the HOPG. B) is used to households the HOPG in the given slot, and sits level into A, with the electrode protruding from the small hole, indicated with red arrow. C) Middle piece of reactor, centre slit provides interaction between HOPG and the counter electrode just above, which is attached onto d) 4 connectors were attached were utilized for pumping electrolyte over the working electrode in a continuous flow. A platinum wire (counter electrode) is fitted parallel to working electrode using a small hole of the piece, indicated by blue arrow.

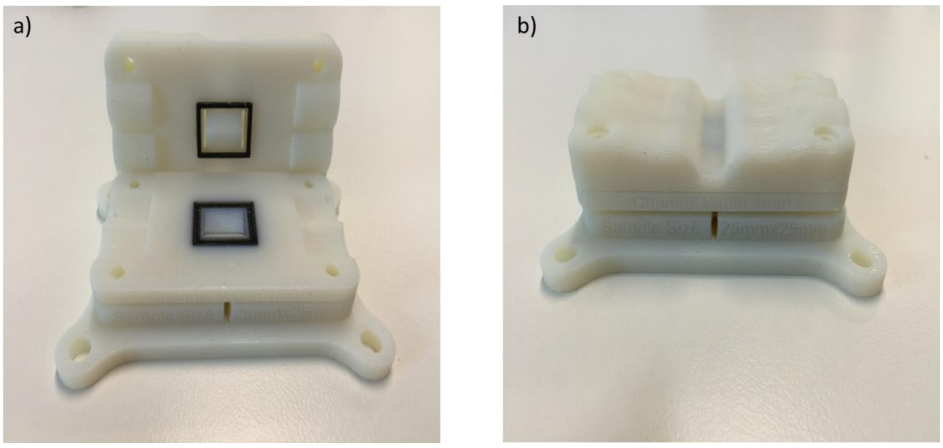

Figure S4: Photo graph of micro reactor after assembling each component precisely.

Before starting the experiment, the micro reactor cell is assembled as shown in figure S1. The reactor consisted of three parts: the top, middle and bottom. The top and bottom portions were used to secure the platinum electrodes, with the top being the counter electrode, and the bottom being the working electrode. These three pieces were assembled together using screws at each corner, and an epoxy to glue the platinum wire in place. Next, the setup was tested for leakage by pumping distilled water through the reactor using a syringe pump. Once all leakage has been resolved, the actual experiments were carried out using only shear, only potential and combination of both as shown in table 1.

S2. Raman Spectroscopy

Raman spectra were obtained using a Renishaw Confocal micro-Raman Spectrometer equipped with a HeNe (632.8 nm) laser operating at 10% power. Extended scans (10 s) were performed between 100 and 3200 wave numbers with a laser spot size of 1 μm. Once the background was removed, the intensity of the spectra was normalized by dividing the data with the maximum intensity. The peak position was found using the full width at half-maximum, as is common practice for analysing spectral data. Each data point reported in figure 4 is collected from at least 8-10 different points for same sample.

S3. Atomic Force Microscopy

Atomic force microscopy measurements were carried out using a JPK Nanowizard 3 to calculate thickness of graphene membranes samples. This instrument is equipped with capacitive sensors to ensure accurate reporting of height, z, and x−y lateral distances. Imaging was performed in tapping mode using Bruker NCHV model cantilevers with diameter 10 nm, with nominal resonant frequencies of 340, *spring* constants of 20−80 N/m. Images were obtained with a set-point force of 1 nN. The cantilever drive frequency was chosen in such a way as to be 5% smaller than the resonance frequency. The thickness of the graphene membrane was estimated from the height difference between the glass and the graphene membrane using a line scan as shown in Fig. 2 and S5.

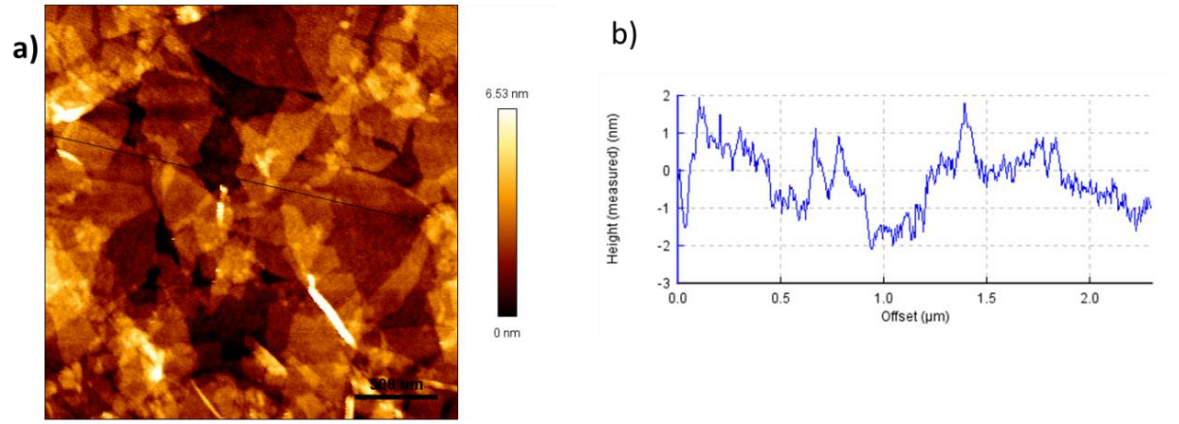

Figure S5: a) AFM measurements of graphene samples synthesized at potential of 6V using shear rate 10^4 s^{-1}, demonstrates smaller size and thicker graphene flakes produced.

S4. Transmission Electron Microscopy

Experimental Details:

Transmission Electron microscopy was carried out by a JEOL JEM 1200 EX operated at an accelerating voltage of 120 kV with a resolution of 3-4 nm. The graphene mostly consists of single- and few-layer sheets. By employing the edge counting method in TEM images taken from several flakes, the number of layers was determined to be less than 4 as shown in figure S6 C. Representative TEM and high-resolution TEM (HR-TEM) images from a single-layer graphene are shown in Figs. S6 a,b. The selected area electron diffraction (SAED; Fig. S6d) illustrates a symmetric six-fold pattern, which refers to graphene.

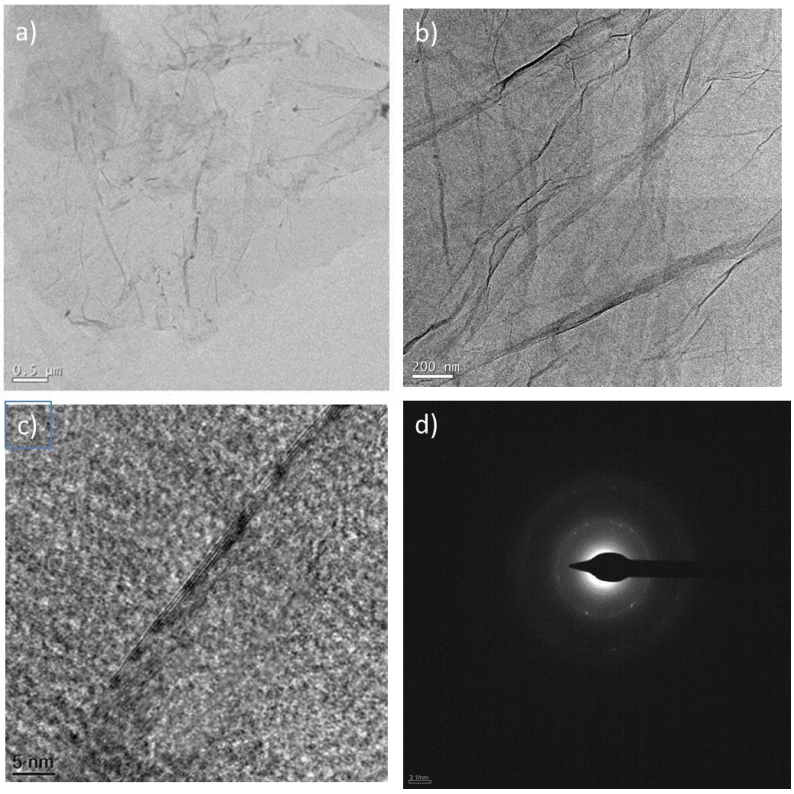

Figure S6: TEM image of monolayer graphene sheet b) tri-layer graphene and c) corresponding fringes pattern and d) electron diffraction pattern with six fold symmetry. Samples prepared at 1V using shear rate of 27500 s^{-1}.

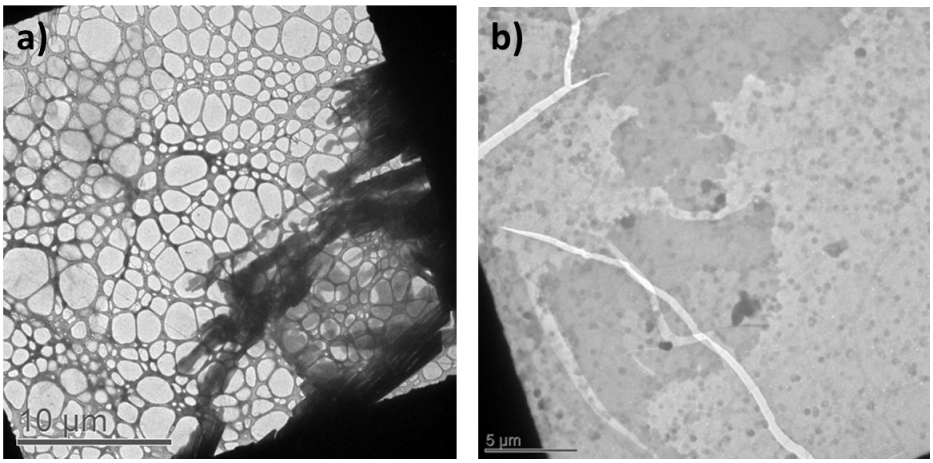

Figure S7: Representative TEM images of graphene using different potential for exfoliation, a) 1 V, and b) 5 V in combination with shear rate 27500 s^{-1}.

S5. The Setup for Tearing Studies of Graphene

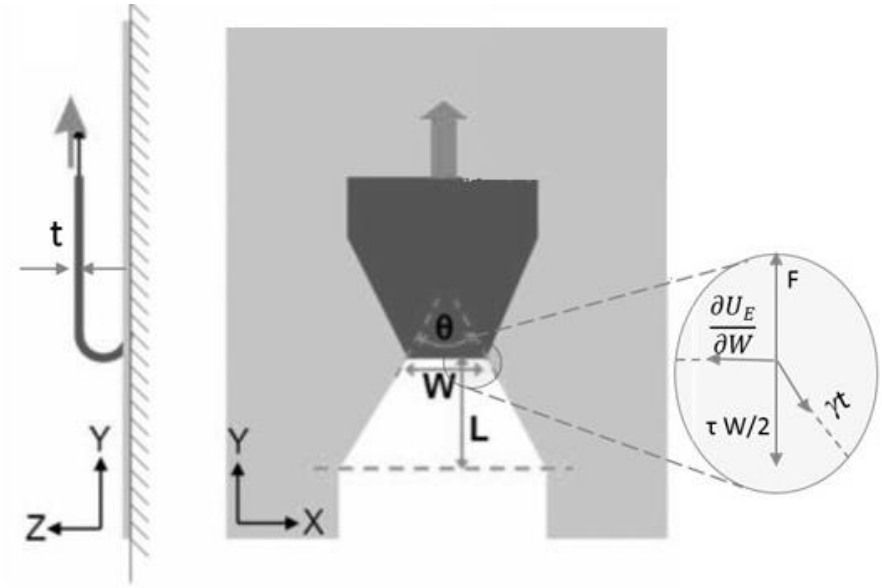

Figure S8: Schematic diagram of the setup for the tearing studies of graphene (reprinted from reference 1).

S6. Optical Images of HOPG (graphite electrode) Before and After Exfoliation

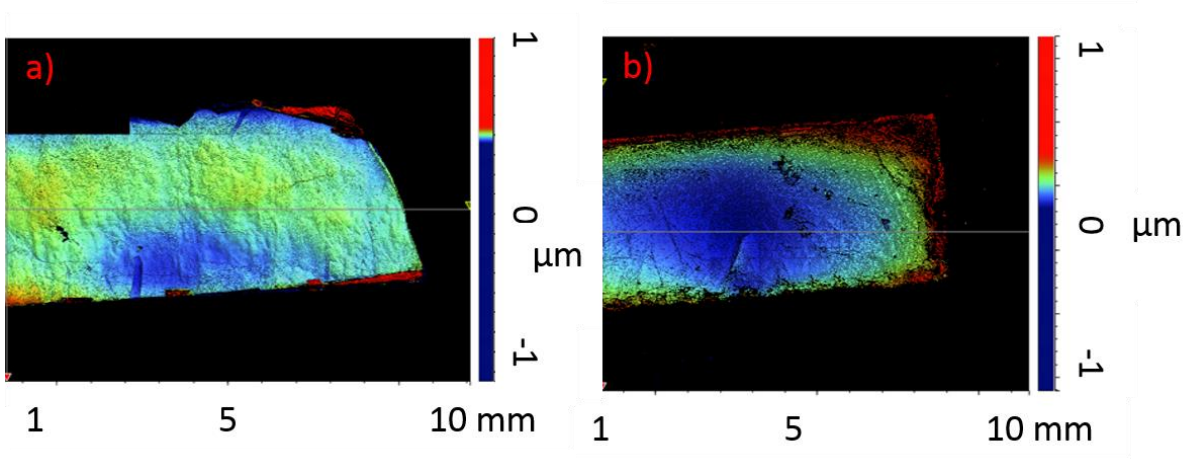

Figure S9: Optical scans of HOPG surface before and after shear driven electrochemical exfoliation experiments, showing the variation in the roughness of the samples from 1.3 to 7.6 micron.

Representative optical images of the working electrode has been taken before and after shear assisted electrochemical exfoliation, implies the variation in the surface roughness, suggesting the effect of exfoliation on the top surface of working electrode.

S7. Dispersion of Exfoliated Graphene in Water and DMF

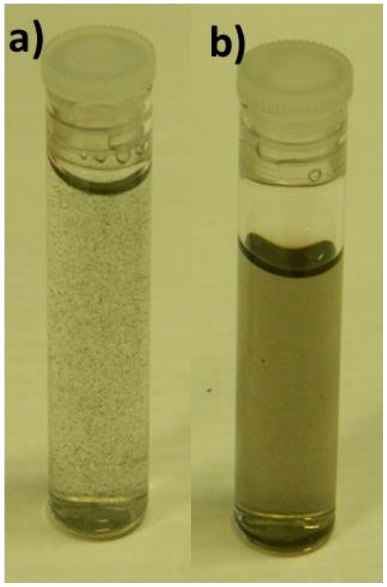

Figure S10: Representative photographs of graphene dispersion, prepared at potential of 1 V and shear rate 10^4 s^{-1} in: a) water, and b) DMF.

The dispersion of graphene in water implies the hydrophobic nature corresponding to less defects and functional groups on the surface. The good dispersion of graphene is due to the solvation effect of DMF, which diminishes the formation of irreversible graphene sheet aggregates.

S8. References

1. D. Sen, K. S. Novoselov, P. M. Reis and M. J. Buehler, *Small*, 2010, **6**, 1108-1116.